

Corrigendum

This corrects parts of:

Screening Supported Amine Sorbents in the Context of Post-combustion Carbon Capture by Vacuum Swing Adsorption, S. Krishnamurthy, J. Boon, C. Grande, A. Lind, R. Blom, R. de Boer, H. Willemsen, G. de Scheemaker, *Chem. Ing. Tech.* **2021**, 93 (6), 929–940. DOI: <https://doi.org/10.1002/cite.202000172>

Eq. 2 should read:

$$\frac{\partial c_i}{\partial t} = -\frac{\partial}{\partial z} \left[c_T D_L \frac{\partial y_i}{\partial z} + c_i v \right] - \frac{(1 - \varepsilon)}{\varepsilon} \frac{\partial \bar{q}_i}{\partial t}$$


In Tabs. 1 and 2, the entry in column 1, line 3 is ΔU_1 [kJ mol⁻¹] and the entry in column 1, line 6 is ΔU_2 [kJ mol⁻¹].

In Tab. 6, *En* of amino silane/SiO₂ at maximum productivity is 1.22 MJ kg⁻¹ (line 6, column 6).

Screening Supported Amine Sorbents in the Context of Post-combustion Carbon Capture by Vacuum Swing Adsorption

Shreenath Krishnamurthy^{1,*}, Jurriaan Boon², Carlos Grande¹, Anna Lind¹, Richard Blom¹, Robert de Boer², Hans Willemsen³, and Gabriel de Scheemaker³

DOI: 10.1002/cite.202000172

 This is an open access article under the terms of the Creative Commons Attribution-NonCommercial-NoDerivs License, which permits use and distribution in any medium, provided the original work is properly cited, the use is non-commercial and no modifications or adaptations are made.



Supporting Information
available online

In Memory of Prof. Dr.-Ing. Jens Weitkamp

The aim of this work was to evaluate the performance of three different supported amine sorbents in a 6-step vacuum swing adsorption (VSA) cycle through process simulation and optimization for a representative post-combustion CO₂ capture system. Detailed process optimization revealed that all the adsorbents were able to achieve the desired purity-recovery targets. The best performing adsorbent in terms of productivity was Lewatit with a productivity of 0.48 mol m⁻³ ads s⁻¹. All the adsorbents exhibited similar minimum specific energy value of around 1 MJ kg⁻¹ on an electric basis.

Keywords: Energy vs productivity Pareto, Post-combustion carbon capture, Process simulation, Supported amine sorbents, Vacuum swing adsorption

Received: July 31, 2020; *revised:* October 29, 2020; *accepted:* February 16, 2021

1 Introduction

The Paris Agreement of 2015 aims to keep the global average temperature below 2 °C from pre-industrial levels [1]. A key action to achieve this goal, is to capture and concentrate the CO₂ from large emission sources such as power plants [2]. In case of power plants, the three major approaches for CO₂ capture are: (1) pre-combustion where the CO₂ is separated prior to the combustion process, (2) post-combustion, in which CO₂ capture is performed after burning the fuel and (3) oxy fuel combustion where the fuel is burnt in the presence of pure oxygen [2]. All three methods give a CO₂ product stream that can be used as carbon source for chemicals (CCU) or permanently stored underground (CCS). Post-combustion capture is particularly advantageous since the capture unit can be retrofitted into existing power plants.

Processes utilizing solid adsorbents, together with absorption using amine solutions [3,4] and membranes [5,6], are the most commonly considered technologies for CO₂ capture. An adsorption process typically relies on the different affinities of a porous solid for different gaseous components. Based on the mode of regeneration, cyclic adsorption processes are classified into pressure swing adsorption (PSA) and temperature swing adsorption (TSA) processes. TSA processes involve heating and cooling of the adsorbent

bed and have long cycle times. Pressure swing adsorption processes cycle between a high pressure and a low pressure. If the PSA process cycles between atmospheric and vacuum pressures, then it is called a vacuum swing adsorption (VSA) process. A typical post-combustion flue gas contains about 15 % CO₂, in case of a coal fired power plant, along with moisture and a large amount of N₂ [7]. Therefore, in this case, a vacuum swing adsorption process that avoids compressing this flue gas with a large amount of nitrogen is more suitable than a PSA process.

Traditionally, PSA processes have been designed for purifying the less strongly adsorbing component, e.g., H₂ purification process [8,9] and gas drying [9]. In the case of CO₂ capture, the main goal is to recover the strongly adsorbed CO₂ in sufficient concentrations. Therefore, this requires an

¹Dr. Shreenath Krishnamurthy, Dr. Carlos Grande, Dr. Anna Lind, Dr. Richard Blom
Shreenath.Krishnamurthy@sintef.no
SINTEF Industry, Forskningsveien 1, Oslo 0373, Norway.

²Dr. Jurriaan Boon, Dr. Robert de Boer
TNO Sustainable Process Technology, P.O. Box 15, 1755 ZG Petten, The Netherlands.

³Hans Willemsen, Gabriel de Scheemaker
3D-cat B.V., Kerkelaan 28, 1861 EB Bergen, The Netherlands.

adsorbent with a high CO₂ selectivity and capacity. Several adsorbents such as zeolites [10–12], activated carbons [13,14], metal-organic frameworks (MOFs) [15,16] and zeolitic imidazolate frameworks (ZIFs) [17,18] are currently being explored for post-combustion CO₂ capture. Amongst these adsorbents, Zeolite 13X is the most widely studied adsorbent due to its commercial availability, low cost and high CO₂ capacity [11,12]. A major drawback of this adsorbent is its hydrophilicity and that the strong adsorption of water affects the adsorption of CO₂ [19,20]. Although it is possible to achieve 95 % CO₂ purity and 90 % CO₂ capture rate at low water concentrations, it is necessary to introduce an initial layer of desiccant in the adsorption column or use a separate column packed with a desiccant in order for the VSA process to operate efficiently at higher moisture contents [21–23]. The presence of water is also detrimental to the CO₂ adsorption in most metal-organic frameworks and in some cases can damage the crystal structure. A classic example is the Mg-MOF-74, which is known to have a very high CO₂ capacity, but is an unstable material showing significant loss in CO₂ capacity with time in the presence of water vapor [24].

To overcome such issues, supported amine sorbents are being explored as potential candidates for post-combustion carbon capture from a wet flue gas. These adsorbents have amine moieties grafted in silica or carbon substrates and are known to exhibit high CO₂ capacities in the presence of water [25–31]. Although these adsorbents are well known to the scientific community for quite some time now, few knowledge gaps still exist. First and foremost, most of the studies are concentrated on equilibrium, adsorption kinetics and stability tests. Very few studies have been carried out to evaluate the performance of supported amine sorbents in the context of a cyclic adsorption processes such as VSA/TSA [31–36]. Therefore, there is not enough information on whether the adsorbent will be able to achieve the DOE targets (95 % purity and 90 % capture rate) and if so, what would the minimum specific energy consumption and the productivity of the adsorption process using these adsorbents. Recent publications from the groups of Farooq and Rajendran have shown that a more reliable way to predict the performance of adsorbents in the context of carbon capture is by performing process simulations and optimization [10,35,37,38]. Through rigorous process optimization, it is possible to identify whether the chosen adsorbent was able to meet the DOE targets. This approach also makes it possible to rank adsorbents that satisfied these targets by means of an energy consumption vs productivity trade-off plot. Secondly, in most of the published work, powdered mesoporous silica like MCM-41 or SBA-15 are used [31]. For the adsorption process to be implemented as a CO₂ capture technology, a large amount of these silica-based materials needs to be synthesized and this might be costly. As an alternative, commercially available silica materials can be used for grafting amine groups onto the silica substrate and there are a few studies using commercially available silica adsorbents [39–41].

In a recent study from our group, we had explored the performance of commercially available silica grafted with an amino silane [42]. This was a multiscale study in which we had performed experiments to obtain the CO₂ and H₂O adsorption isotherms and detail process optimization using the isotherm data for identifying optimum operating conditions. From this study, we had seen that it was indeed possible to obtain 95 % CO₂ purity and 90 % CO₂ recovery using our sorbent, in a 6-step VSA cycle.

The aim of the present work is to compare our adsorbent with two other supported amine sorbents. One adsorbent is Lewatit VP OC 1065 containing a primary benzyl amine group. The other adsorbent is a commercial silica grafted with PEI (polyethyleneimine). The adsorption isotherms of the latter two adsorbents were obtained from literature. The first step was to perform detailed process optimization by genetic algorithm to identify the operating conditions at minimum specific energy and maximum productivity. The adsorbents were then ranked based on the productivity vs specific energy trade-off plots. The next step was to identify any relationship between the performance of the adsorbents and the two isotherm characteristics, namely CO₂ capacity and isotherm nonlinearity. These results will be discussed in the subsequent sections.

2 Materials

The three supported amine sorbents that will be evaluated are Lewatit VP OC 1065 (Lewatit), and two other silica sorbents grafted with polyethyleneimine (PEI/SiO₂) and N-[3-(trimethoxysilyl)propyl]ethylenediamine (amino silane/SiO₂). Data for CO₂ and H₂O isotherms for the first two adsorbents are extracted from the work of Veneman et al. [29] and Dijkstra et al. [41] using the web plot digitizer software. The amino silane grafted silica adsorbent was characterized at SINTEF. CO₂ isotherms were measured for 70, 90 and 110 °C while H₂O isotherms were measured for 70, 80 and 90 °C. The data is reported in a previous publication [42]. Both in our work and in that of Dijkstra et al. [41] PERL-KAT mesoporous silica was used. The isotherms of CO₂ in all materials were fitted to a dual site Langmuir model shown below.

$$q_i^* = \frac{q_{s1} b_{01} e^{-\frac{\Delta U_1}{RT} c_i}}{1 + b_{01} e^{-\frac{\Delta U_1}{RT} c_i}} + \frac{q_{s2} b_{02} e^{-\frac{\Delta U_2}{RT} c_i}}{1 + b_{02} e^{-\frac{\Delta U_2}{RT} c_i}} \quad (1)$$

Where, q_{s1} and q_{s2} are the saturation capacities, b_{01} and b_{02} are the pre-exponential Langmuir constants and ΔU_1 and ΔU_2 are the internal energies of the two sites. Since the isotherms in the work of Dijkstra et al. [41] were only measured up to 0.2 bar, we have fitted CO₂ isotherms by fixing the total saturation capacity of the two sites to be 2.3 mmol g⁻¹. The saturation capacity was obtained from the work of Sutanto et al. [43] who had used a similar adsorbent. For the other sorbents, no such constraints were imposed. As the H₂O isotherms were linear, the saturation

capacities were fixed to be that of CO_2 and only the b and ΔU values were fitted.

The isotherms of CO_2 and H_2O at 90°C are shown in Fig. 1 and the corresponding isotherm parameters are shown Tabs. 1 and 2. The order of CO_2 capacity at 0.15 bar in these adsorbents are $\text{PEI} > \text{Lewatit} > \text{amino silane}$. The corresponding capacity values are 1.4, 1.2 and 0.73 mmol g^{-1} , respectively.

The H_2O adsorption capacities were similar in PEI and amino silane grafted silica as shown in Fig. 1b. In the case of Lewatit, Veneman et al. [29] reported isotherm data at 30, 40 and 75°C . For the sake of consistency, we have used the H_2O isotherm data on amino silane and scaled appropriately to match the H_2O adsorption isotherm on Lewatit at 75°C . This isotherm was then used in the process simulations. The adsorption isotherm parameters are reported in Tabs. 1 and 2.

The adsorption of nitrogen in the amino silane grafted silica was negligible under these conditions [42]. Nitrogen is

also considered non-adsorbing in PEI grafted sorbents and Lewatit [34, 44].

3 Vacuum Swing Adsorption Process

In this study a 6-step vacuum swing adsorption (VSA) process was chosen to evaluate the different amine groups. This cycle has already been studied by Khurana and Farooq [10]. The schematic of the 6-step VSA process is shown in Fig. 2. The cycle consists of the following steps:

- 1) Adsorption with feed: This step takes place at a high pressure P_H . Feed is introduced to the column from the feed end (bottom). Preferential adsorption of CO_2 and H_2O takes place and the light product N_2 is collected at the product end (top), at ambient pressure.
- 2) Rinse step: In this step, the column is purged with a stream that is rich in heavy product CO_2 and the light product is collected at the product end. The purpose of this step is to enhance the CO_2 purity. The heavy reflux step is carried out with a stream from the subsequent light reflux step. Therefore, the duration is the same as that of the light reflux step.
- 3) Cocurrent evacuation: The feed end is closed, and the column is evacuated to an intermediate pressure P_{INT} from the product end to remove the nitrogen that is remaining in the column. This step also aids in improving the product purity.
- 4) Countercurrent evacuation: The column is evacuated in the countercurrent direction to remove the adsorbed CO_2 . Here the column is evacuated to the low pressure P_L .
- 5) Light reflux: The column is purged with a part of the adsorption product to remove the remaining CO_2 the column. The entirety of this stream is recycled back to the column in the rinse step. This step also takes place at the low pressure P_L . Since this step is carried out with the adsorption product, the duration of this step cannot be greater than the adsorption step.
- 6) Light product pressurization: Finally, the column is pressurized to P_H with the light product of the adsorption step in the countercurrent direction.

3.1 Modeling of the Vacuum Swing Adsorption Process

A non-isothermal, non-isobaric model based on the following assumptions is used:

- 1) axial dispersion is considered,
- 2) no radial temperature or concentration gradients,

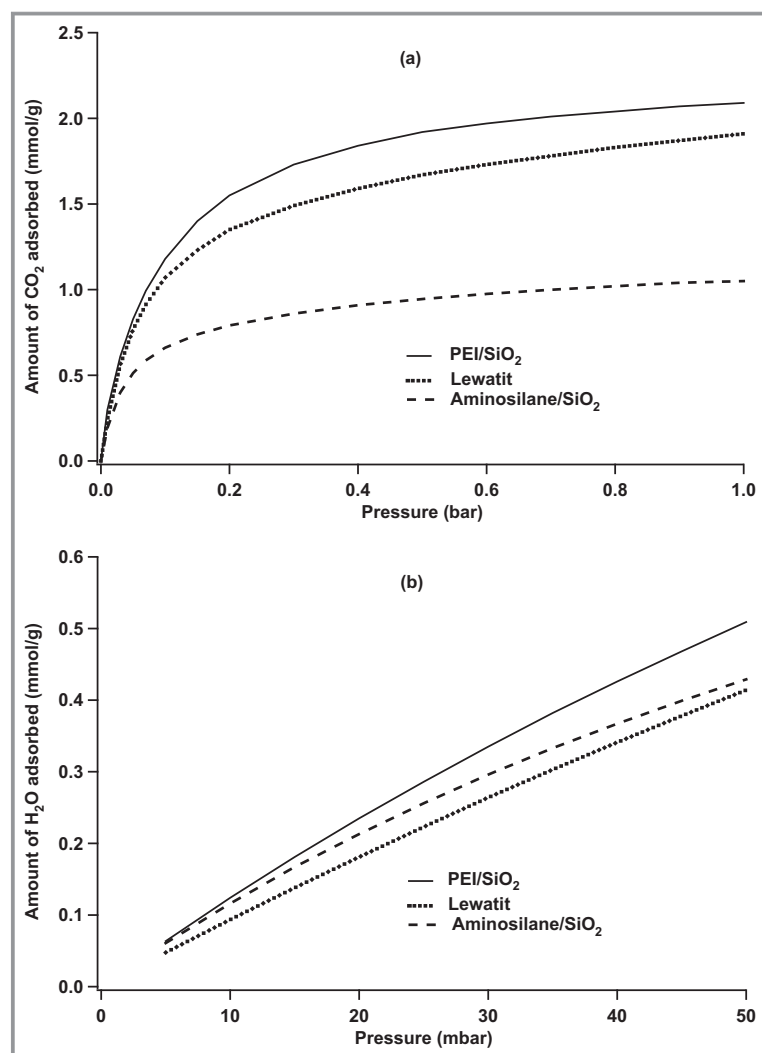


Figure 1. a) CO_2 and b) H_2O isotherms in the different supported amine sorbents at 90°C .

Table 1. CO₂ adsorption isotherm parameters for different supported amine sorbents

Parameter	Amino silane	Lewatit VP OC	PEI/SiO ₂	PEI_A2
q_{s1} [mmol g ⁻¹]	0.8	1.54	2.12	1.92
$b_{0,1}$ [mol m ⁻³]	$2.7 \cdot 10^{-16}$	$3.7 \cdot 10^{-13}$	$5.7 \cdot 10^{-16}$	$9.8 \cdot 10^{-15}$
$-\Delta U_1$ [kJ mol ⁻¹]	-107.8	-84.7	-102.1	-95.2
q_{s2} [mmol g ⁻¹]	0.5	1.33	0.18	1.8
$b_{0,2}$ [mol m ⁻³]	$6.5 \cdot 10^{-9}$	$2.5 \cdot 10^{-11}$	$3.11 \cdot 10^{-6}$	$7.9 \cdot 10^{-9}$
$-\Delta U_2$ [kJ mol ⁻¹]	-46.7	-61.01	-43.8	-40.35
q_0 (0.15 bar, 90 °C) [mmol g ⁻¹]	0.73	1.2	1.4	1.4
Nonlinearity λ (q_0/q_s)	0.56	0.42	0.61	0.37

- ideal gas law is valid,
- the adsorbent properties are uniform throughout the column,
- instantaneous thermal equilibrium between gas and solid phases,
- uniform porosity throughout the column.

The model equations are a set of coupled partial differential equations, which are given below.

Component mass balance:

$$\frac{\partial c_i}{\partial t} = -\frac{\partial}{\partial z} \left[c_T D_L \frac{\partial y_i}{\partial t} + c_i v \right] - \frac{(1-\varepsilon)}{\varepsilon} \frac{\partial \bar{q}_i}{\partial t} \quad (2)$$

By applying ideal gas law $c = P/(RT)$ Eq. (2) becomes

Table 2. H₂O adsorption isotherm parameters for different supported amine sorbents.

Parameter	Amino silane	Lewatit VP OC	PEI/SiO ₂	PEI_A2
q_{s1} [mmol g ⁻¹]	0.8	1.54	2.12	1.92
$b_{0,1}$ [mol m ⁻³]	$1.5 \cdot 10^{-6}$	$1.88 \cdot 10^{-6}$	$1.1 \cdot 10^{-10}$	$1.2 \cdot 10^{-10}$
$-\Delta U_1$ [kJ mol ⁻¹]	-36.8	-32.9	-63.9	-61.9
q_{s2} [mmol g ⁻¹]	0.5	1.33	0.18	1.8
$b_{0,2}$ [mol m ⁻³]	$1.5 \cdot 10^{-6}$	$1.88 \cdot 10^{-6}$	$1.1 \cdot 10^{-10}$	$1.6 \cdot 10^{-10}$
$-\Delta U_2$ [kJ mol ⁻¹]	-36.8	-32.9	-63.9	-61.1
q_0 (0.05 bar, 90 °C) [mmol g ⁻¹]	0.48	0.41	0.5	0.5

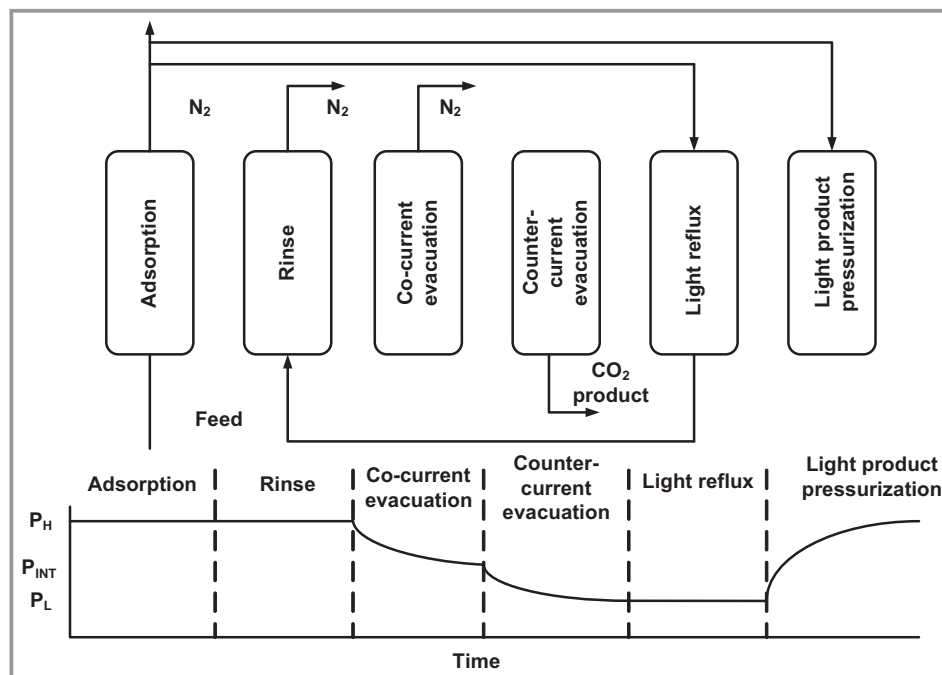
$$\frac{\partial y_i}{\partial t} + \frac{y_i}{P} \frac{\partial P}{\partial t} - \frac{y_i}{T} \frac{\partial T}{\partial t} = \frac{T}{P} D_L \frac{\partial \left(\frac{P}{T} \frac{\partial y_i}{\partial z} \right)}{\partial z} - \frac{T}{P} \frac{\partial \left(\frac{y_i P}{T} v \right)}{\partial z} - \frac{RT}{P} \frac{(1-\varepsilon)}{\varepsilon} \frac{\partial \bar{q}_i}{\partial t} \quad (3)$$

The overall mass balance equation is given by

$$\frac{1}{P} \frac{\partial P}{\partial t} - \frac{1}{T} \frac{\partial T}{\partial t} = -\frac{T}{P} \frac{\partial \left(\frac{P}{T} v \right)}{\partial z} - \frac{(1-\varepsilon)}{\varepsilon} \frac{RT}{P} \sum_{i=1}^n \frac{\partial \bar{q}_i}{\partial t} \quad (4)$$

As mentioned earlier, the mass transfer between the gas and the solid phases was described by linear driving force approximation, which is of the following form:

$$\frac{\partial \bar{q}_i}{\partial t} = k_i (q_i^* - \bar{q}_i) \quad (5)$$

**Figure 2.** Schematic of the 6-step VSA cycle.

where, k_i is the linear driving force (LDF) coefficient and q_i^* is the equilibrium solid phase concentration.

The column energy balance and the wall temperature balance equations are as follows:

$$\left[\frac{(1-\varepsilon)}{\varepsilon} \left(\rho_s C_{ps} + C_{pa} \sum_{i=1}^n \bar{q}_i \right) \right] \frac{\partial T}{\partial t} = \frac{k_z}{\varepsilon} \frac{\partial^2 T}{\partial z^2} - \frac{C_{pg}}{R} \frac{\partial(vP)}{\partial z} - \frac{C_{pg}}{R} \frac{\partial P}{\partial t} + \frac{(1-\varepsilon)}{\varepsilon} \sum_{i=1}^n (-\Delta H_i - C_{pa} T) \frac{\partial \bar{q}_i}{\partial t} - \frac{2h_i}{\varepsilon r_i} (T - T_w) \quad (6)$$

$$\rho_w C_{pw} \frac{\partial T_w}{\partial t} = k_w \frac{\partial^2 T_w}{\partial z^2} + \frac{2r_i h_i}{r_o^2 - r_i^2} (T - T_w) - \frac{2r_o h_o}{r_o^2 - r_i^2} \times (T_w - T_a) \quad (7)$$

The pressure drop across the column was described by Blake Kozeny equation [45].

$$-\frac{\partial P}{\partial z} = \frac{180}{4r_p^2} \left(\frac{1-\varepsilon}{\varepsilon} \right)^2 \mu v \quad (8)$$

Rearranging Eq. (8) gives the local velocity

$$v = \frac{4}{180\mu} \left(\frac{\varepsilon}{1-\varepsilon} \right)^2 r_p^2 \left(-\frac{\partial P}{\partial z} \right) \quad (9)$$

The set of model equations has been used in earlier studies [23, 35, 46, 47] and the model was validated using pilot plant experimental data of Krishnamurthy et al. [48]. The model equations are converted to dimensionless form by using appropriate dimensionless variables, the details of which are provided in the Supporting Information (SI).

3.2 Process Performance Indicators

The performance of the process is quantified by the following performance indicators namely:

$$\text{Purity} = \frac{\text{moles}_{\text{CO}_2, \text{cn-evac}}}{\text{moles}_{\text{total, cn-evac}} - \text{moles}_{\text{H}_2\text{O, cn-evac}}} \quad (10)$$

In case of a wet flue gas, the purity is reported on a dry basis and therefore the moles of H₂O obtained in the evacuation step is subtracted from the total moles in the evacuation step.

$$\text{Recovery} = \frac{\text{moles}_{\text{CO}_2, \text{cn-evac}}}{\text{moles}_{\text{CO}_2, \text{fed}}} \quad (11)$$

Recovery determines the rate of CO₂ capture and is the ratio of the amount of CO₂ captured to the amount of CO₂ in the feed.

$$\text{Productivity} = \frac{\text{moles}_{\text{CO}_2, \text{cn-evac}}}{\text{Volume of adsorbent} \times \text{cycle time}} \quad (12)$$

Productivity is an indicator of the footprint of the capture unit. Higher the productivity, smaller is the footprint.

$$\text{Specific energy} = \frac{\text{Energy}_{\text{vacuum}} + \text{Energy}_{\text{compression}}}{\text{Moles}_{\text{CO}_2, \text{cn-evac}}} \quad (13)$$

The energy consumption of the vacuum pumps was calculated assuming 72 % efficiency using Eq. (14) [49]

$$\text{Energy}_{\text{vacuum}} = \frac{1}{\eta} \varepsilon \pi r_i^2 \frac{\gamma}{\gamma - 1} \int_{t=0}^{t=t_{\text{vacuum}}} v P \left[\left(\frac{P_{\text{atm}}}{P(t)_{\text{vacuum}}} \right)^{\frac{\gamma}{\gamma-1}} - 1 \right] dt \quad (14)$$

For each individual step, appropriate boundary conditions have been used and these are given in the SI. The initial conditions of a given step are the final conditions of the previous step. The simulations are carried out till cyclic steady-state condition, i.e., the mass balance error for three consecutive cycles is less than 0.6 %. The maximum number of cycles was kept to 200.

3.3 Process Simulation and Optimization

To obtain the numerical solution, the non-dimensional model equations were discretized in the spatial domain and converted to a set of differential algebraic equations using the finite volume method. Finite volume numerical method has been found to be robust and less intensive in terms of computational time [47, 50]. It is also capable of handling sharp fronts encountered in case of CO₂ adsorption and providing non-oscillatory solutions [47, 50]. The system of differential algebraic equations was then numerically solved using ode15s solver in Matlab.

The 6-step VSA cycle simulation was first validated with the results from Khurana and Farooq [10]. The next step was to perform detailed process optimization to rank these adsorbents in terms of specific energy and productivity. The ranking is based on identifying the minimum specific energy and maximum productivity subject to 95% CO₂ purity and 90% CO₂ recovery targets. In case of the 6-step VSA process, there are seven key variables or decision variables that affect the process performance. These variables are adsorption step time, reflux time, cocurrent and countercurrent evacuation step times, interstitial feed velocity and the cocurrent and countercurrent evacuation pressures. In order to identify the operating conditions corresponding to the minimum specific energy and maximum productivity, the 6-step VSA cycle was optimized rigorously using genetic algorithm. Genetic algorithm for VSA optimization is widely studied in literature [35, 46, 51, 52] and we have used the inbuilt multi objective optimization function in Matlab, gamultiobj, which is based on the non-dominated sorting genetic algorithm (NSGA-II) of Deb et al. [53].

A feed gas containing 15% CO₂, 5% H₂O and 80% N₂ was considered. The feed temperature was 90 °C. The choice of the feed temperature is based on our previous study where we had seen that our amine grafted sorbent performed better in VSA process at 90 °C than at 70 °C [42]. The amount of water in the feed is restricted to 5 % owing to the limitations in the experimental setup where it was possible to measure isotherms only up to 4.2 kPa. The input parameters for the simulations are summarized in Tab. 3. The expression for the LDF coefficient reported in Tab. 3 was obtained from breakthrough experiments carried out with the amino-silane adsorbent and the details of the breakthrough experiments are provided in another publication [42].

Table 3. Input parameters for the process simulation.

Parameter	Value
Length of column [m]	1
Internal diameter [m]	0.1
External diameter [m]	0.11
Column void fraction [-]	0.37
Adsorbent pellet density [kg m ⁻³]	1052
Adsorbent specific heat [J kg ⁻¹ K ⁻¹]	1700
Diameter of pellets [mm]	2
Internal heat transfer coefficient [W m ⁻² K ⁻¹]	0
External heat transfer coefficient [W m ⁻² K ⁻¹]	0
Specific heat of the gas mixture [J kg ⁻¹ K ⁻¹]	1054
LDF co-efficient of CO ₂ [s ⁻¹]	10 ⁶ e ^{-6415/T}

In total, 7000 simulations were performed for each adsorbent using genetic algorithm with the upper and lower bounds of the decision variables given in Tab. 4. The objective functions are

$$\text{Obj}_1 = \frac{\text{Specific energy}}{100} + 10000 \max\left(0, 0.95 - \frac{\text{CO}_2 \text{ purity}}{100}\right)^2 + 10000 \max\left(0, 0.9 - \frac{\text{CO}_2 \text{ capture rate}}{100}\right)^2 \quad (15)$$

Table 4. Upper and lower bounds for the decision variables.

Variable	Adsorption time [s]	Cocurrent evacuation time [s]	Reflux step time [s]	Counter current evacuation time [s]	Cocurrent evacuation pressure P_1 [bar]	Counter current evacuation pressure P_L [bar]	Feed velocity V_0 [m s ⁻¹]
Lower bound	10	10	1	10	0.1	0.1	0.1
Upper bound	300	300	100	300	0.5	0.5	3

$$\text{Obj}_2 = \frac{1}{\text{Productivity}} + 10000 \max\left(0, 0.95 - \frac{\text{CO}_2 \text{ purity}}{100}\right)^2 + 10000 \max\left(0, 0.9 - \frac{\text{CO}_2 \text{ capture rate}}{100}\right)^2 \quad (16)$$

Once the optimization was complete, productivity vs specific energy Pareto fronts were obtained, corresponding to 95 % purity and 90 % recovery. These Pareto fronts were then used to rank these adsorbents.

4 Results and Discussion

Fig. 3 shows the Pareto fronts for the three different adsorbents. All the points on the Pareto fronts for the different adsorbents satisfy the 95 % purity on a dry basis and 90 % recovery constraints. The specific energy consumption reported in this work is on an electric basis. Each point on the Pareto front corresponds to different values of the decision variables. As mentioned earlier, the simulations were carried out till cyclic steady state (CSS). This means that the mass balance error, defined below between three consecutive cycles is less than 0.6 %

$$\text{Mass balance error} = \left| \frac{\text{moles}_{in} - \text{moles}_{out}}{\text{moles}_{in}} \right| * 100 \quad (17)$$

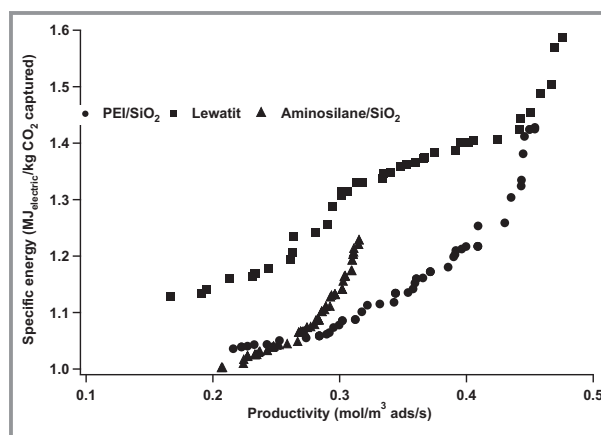


Figure 3. Specific energy vs productivity Pareto fronts for the different sorbents.

From the Pareto fronts it can be seen that the amino silane grafted silica had the lowest productivity and the productivity values ranged from 0.21–0.32 mol m⁻³ adsorbent s⁻¹. PEI grafted silica exhibited productivity values between 0.2–0.45 mol m⁻³ adsorbent s⁻¹, while Lewatit had a productivity ranging from 0.17–0.48 mol m⁻³ adsorbent s⁻¹. Therefore, from this it is evident that the best performing adsorbent in terms of productivity is Lewatit. Fig. 4 shows the feed flow rate (interstitial velocity) with respect to the productivity. In case of Lewatit and PEI grafted silica, the optimizer chose a higher flow rates in comparison with the amino silane grafted silica sorbent. This can be attributed to the high CO₂ capacity in the two sorbents over the amino silane grafted silica, thereby resulting in improved productivity.

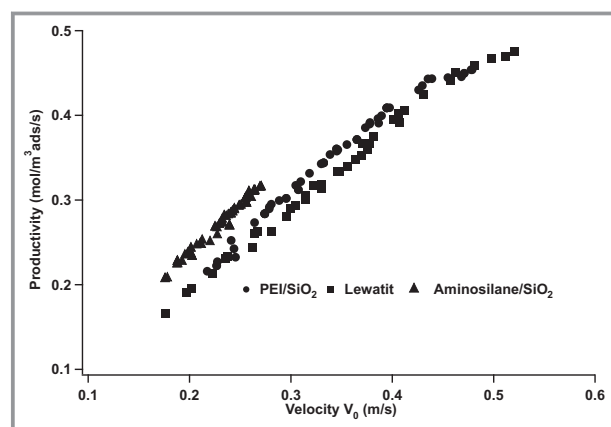


Figure 4. Interstitial velocity vs productivity.

The minimum specific energy was 1 MJ kg⁻¹ electric for the amino silane grafted sorbent. For PEI grafted silica and Lewatit the minimum specific energy values were 1.04 and 1.13 MJ kg⁻¹, respectively. The operating conditions and the energy consumption in the various steps are shown in Tabs. 5 and 6. The higher minimum specific energy of Lewatit can be attributed to the fact that the amount of CO₂ fed was also lower, although the energy consumed by the vacuum pumps and compressors were the lowest for this adsorbent at the minimum specific energy consumption.

From Tab. 6, it can be seen that the bulk of the energy consumption in the VSA process comes from the light reflux and the countercurrent evacuation steps. These two steps contribute to about 98 % of the energy consumption in the 6-step VSA cycle and the remaining steps contribute to the remaining 2 %. The specific energy consumption versus the energy consumption in the light reflux step and the evacuation step are shown in Fig. 5. Looking at Eq. (5) we can interpret that the energy consumption is a function of the pressure ratio and the flowrate to the vacuum pumps. Higher the flowrate, higher is the energy consumed by the vacuum pumps. The maximum energy consumptions in the light reflux steps were 95 kJ, 68 kJ and 48 kJ for Lewatit, PEI/SiO₂ and amino silane/SiO₂, respectively. For the evacuation steps, these values were 31 kJ, 25 kJ and 15 kJ for Lewatit, PEI/SiO₂ and amino silane/SiO₂, respectively. At specific energy values of below 1.4 MJ kg⁻¹ Lewatit performed better than PEI, which is result of the low pressure values chosen by the optimizer. In case of Lewatit the values were between than 0.14–0.22 bar, whereas for PEI, the value was 0.14 bar or less. At the highest energy consumption values, where the productivity was maximum, the optimizer chose an evacuation pressure closer to the lower bound of 0.1 bar as seen from Fig. 6.

It should be noted that although PEI/SiO₂ had the highest capacity, the maximum productivity was 0.45 mol m⁻³ ads s⁻¹ as opposed to 0.48 mol CO₂ m⁻³ ads s⁻¹ of Lewatit. This we suspect could be due to the high nonlinearity of CO₂ isotherm in PEI/SiO₂, which is a result of fixing the saturation capacity. The isotherm nonlinearity is defined as the ratio of the adsorption capacity at the feed conditions to the saturation capacity ($\lambda = q_0/q_s$). Nonlinearity is a measure of the shape of the isotherm, an isotherm with a nonlinearity value of 1 is considered rectangular and a nonlinearity close to 0 is considered linear. With respect to this work, the values of nonlinearity were 0.42, 0.57 and 0.61 for Lewatit, amino silane/SiO₂ and PEI/SiO₂, respectively.

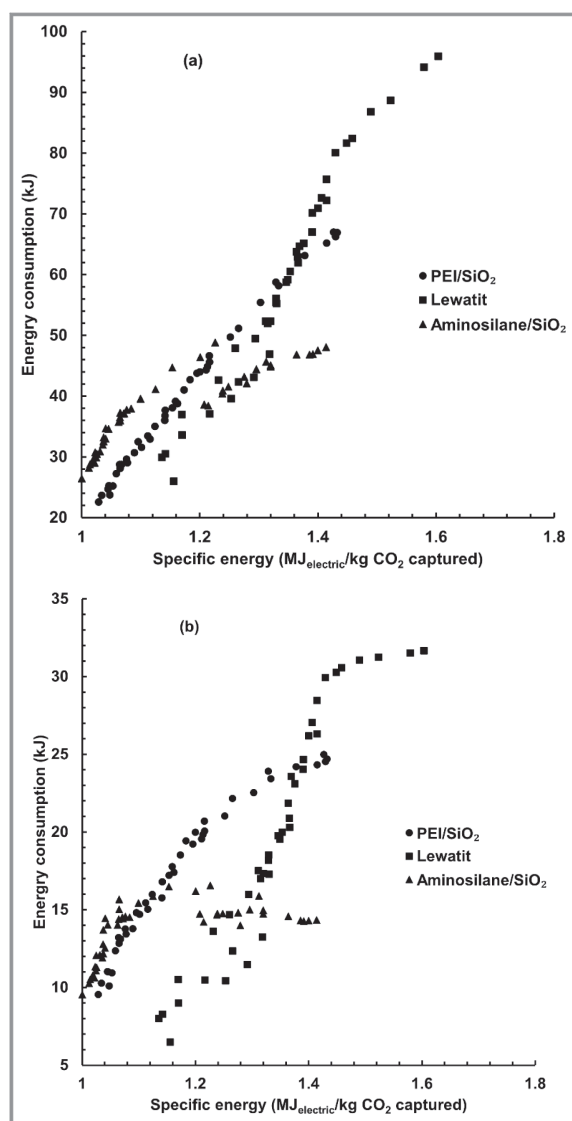
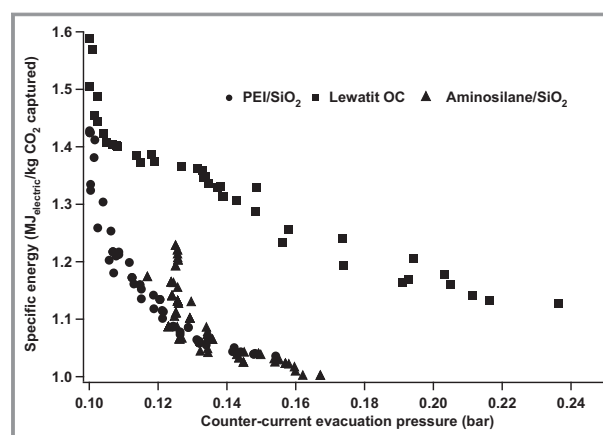
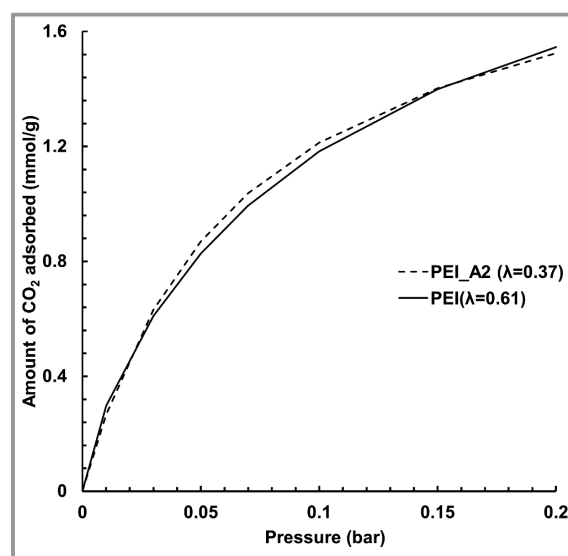
A different set of isotherm parameters was obtained when the total saturation capacity was not fixed and is shown in Tab. 2. The isotherms are plotted in Fig. 7 and these isotherms have different shapes but the capacity at 0.15 bar is

Table 5. Operating conditions for the minimum specific energy and maximum productivity conditions for the different adsorbents.

Operating configuration	Sorbent	t_{ads} [s]	$t_{\text{co-evac}}$ [s]	$t_{\text{cn-evac}}$ [s]	t_{reflux} [s]	P_{INT} [bar]	P_L [bar]	V_0 [m s ⁻¹]	CO ₂ fed [m ³]	Cycle time [s]
Minimum specific energy	Lewatit OC	70.66	25.28	55.11	24.75	0.36	0.24	0.18	0.02	210.54
	PEI/SiO ₂	62.47	28.90	45.28	14.37	0.33	0.15	0.22	0.02	175.39
	Amino silane/SiO ₂	89.42	24.75	42.77	22.00	0.34	0.17	0.18	0.03	210.94
Maximum productivity	Lewatit OC	66.13	25.02	53.63	25.54	0.40	0.10	0.52	0.06	205.85
	PEI/SiO ₂	57.96	28.23	39.54	19.17	0.35	0.10	0.48	0.05	174.06
	Amino silane/SiO ₂	84.45	25.26	34.67	25.18	0.37	0.13	0.27	0.04	204.73

Table 6. Performance indicators at the minimum specific energy and maximum productivity conditions.

Operating configuration	Sorbent	Pu [%]	Re [%]	Prod [mol m ⁻³ ads s ⁻¹]	En [MJ kg ⁻¹]	W_{ads} [kJ]	$W_{co-evac}$ [kJ]	$W_{cn-evac}$ [kJ]	W_{Rinse} [kJ]	W_{LR} [kJ]	W_{total} [kJ]
Minimum specific energy	Lewatit OC	96.47	91.03	0.17	1.13	0.07	0.51	6.47	0.24	25.97	33.26
	PEI/SiO ₂	95.05	90.23	0.22	1.04	0.09	0.56	9.80	0.17	23.40	34.01
	Amino silane/SiO ₂	95.84	90.17	0.21	1.00	0.09	0.53	9.42	0.19	26.17	36.40
Maximum productivity	Lewatit OC	96.02	90.15	0.48	1.59	0.56	0.42	31.6	1.25	95.94	129.8
	PEI/SiO ₂	96.82	90.25	0.45	1.43	0.42	0.55	25.40	0.81	68.84	95.80
	Amino silane/SiO ₂	95.98	91.12	0.32	0.00	0.2	0.61	14.6	0.44	48.08	63.9

**Figure 5.** The energy consumption in the a) light reflux step and b) countercurrent evacuation steps with respect to the specific energy consumption of the process.**Figure 6.** Specific energy as a function counter-current evacuation pressure.**Figure 7.** Isotherms with different saturation capacities.

the same. This isotherm had a nonlinearity parameter of 0.37. With the resultant parameters the optimization was repeated and this time the performance was better in terms of specific energy and productivity as seen from Fig. 8. The maximum productivity and minimum specific energy values were $0.5 \text{ mol m}^{-3} \text{ ads s}^{-1}$ and 1.03 MJ kg^{-1} . This increase in productivity was attributed to the increased amount of CO_2 treated, as seen from Fig. 9.

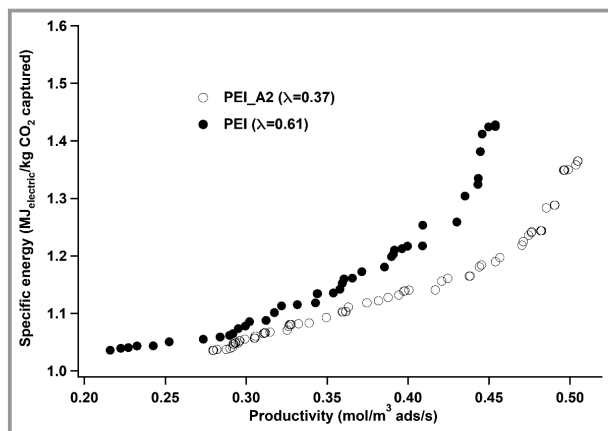


Figure 8. Specific energy vs productivity Pareto fronts for different sorbents.

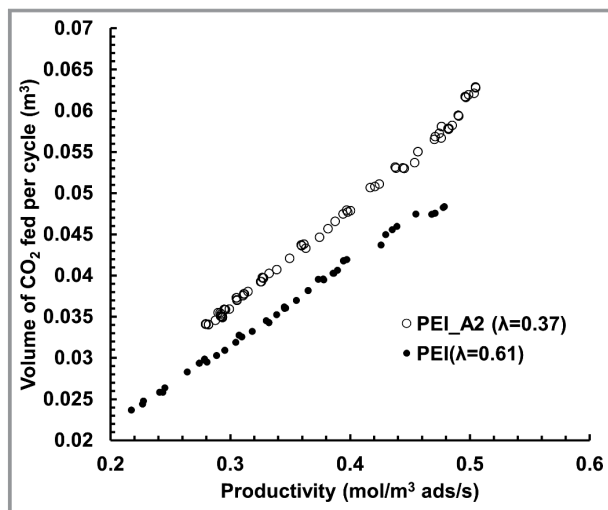


Figure 9. Amount of CO_2 fed with respect to the productivity in case of PEI/ SiO_2 .

From this exercise it is clear that the fitting of isotherms plays a key role in predicting the performance of an adsorbent. In case of the work of Dijkstra et al. [41] the isotherms were only measured up to 0.2 bar and, thus, saturation capacity had to be fixed based a follow up work. Therefore, it is recommended that isotherms are measured up to 1 bar pressure, to avoid uncertainties in the estimation of saturation capacities. One may also consider low temperatures below ambient conditions to obtain capacities close to satu-

ration at 1 bar, but this may not be suitable for supported amine sorbents due to their slow adsorption kinetics. A more challenging but more rewarding application would be to the use of molecular simulation tools to obtain the isotherms of the various constituents up to 1 bar and at various temperatures.

Through this exercise of isotherm fitting, it was also shown that there is an effect of the nonlinearity on the process performance. We acknowledge that about 11% improvement in productivity was possible, and may not be significant. Nevertheless, the effect could be more pronounced as the adsorption isotherm becomes closer to being rectangular i.e., nonlinearity close to 1. In such a scenario, the 6-step VSA cycle may have to operate at lower vacuum of < 0.1 bar to achieve the desired recovery and this would increase the energy consumption and as well as affect the productivity values.

Fig. 10 shows the temperature profiles along the column for the three different adsorbents. The temperature swing is maximum in case of the amino silane grafted silica, which had the highest heat of adsorption of -111 kJ mol^{-1} . The maximum temperature observed at the cyclic steady-state condition is around 125°C . The stability of this material with respect to temperature was not studied, but we suspect that the CO_2 adsorption capacity would be affected over time if such temperatures are attained in the process. The high heat of adsorption also explains the spread in the CO_2 concentration profile in case of amino silane sorbent as seen in Fig. S3. As expected, Lewatit with the lowest heat of adsorption of -87 kJ mol^{-1} exhibited the lowest temperature swing, and the maximum temperature was around 110°C . The sorbent is reported to be stable up to 130°C , after which formation of urea may take place [34]. In case of PEI, the maximum temperature is around 120°C and like Lewatit this sorbent is also stable up to 130°C in the presence of the CO_2 and H_2O [43]. In this study, the presence of oxygen was not considered, i.e., the oxygen has been modeled along with nitrogen. The presence of oxygen in the flue gas could be detrimental for the supported amine sorbents at higher temperatures $> 100^\circ\text{C}$ [54] and, therefore, it is necessary to design cyclic processes with due consideration to sorbent stability as well as the kinetics.

We have also carried out tests to ensure the consistency of the Pareto fronts generated for this study. In the first step, the output from the process optimization was periodically monitored and the Pareto front was plotted for every thousand simulations. The evolution of the Pareto front is shown in Fig. S1 of the SI and it can be seen that there is minimal change in the two objectives, i.e., minimum specific energy and maximum productivity after 4000 simulations. The optimization for one of the cases (PEI_A2) was repeated to verify the reproducibility of the results from the process optimization. The resultant Pareto front is shown in Fig. S2 of the SI. The differences in the two objectives minimum specific energy and maximum productivity were 2% and 4%, respectively.

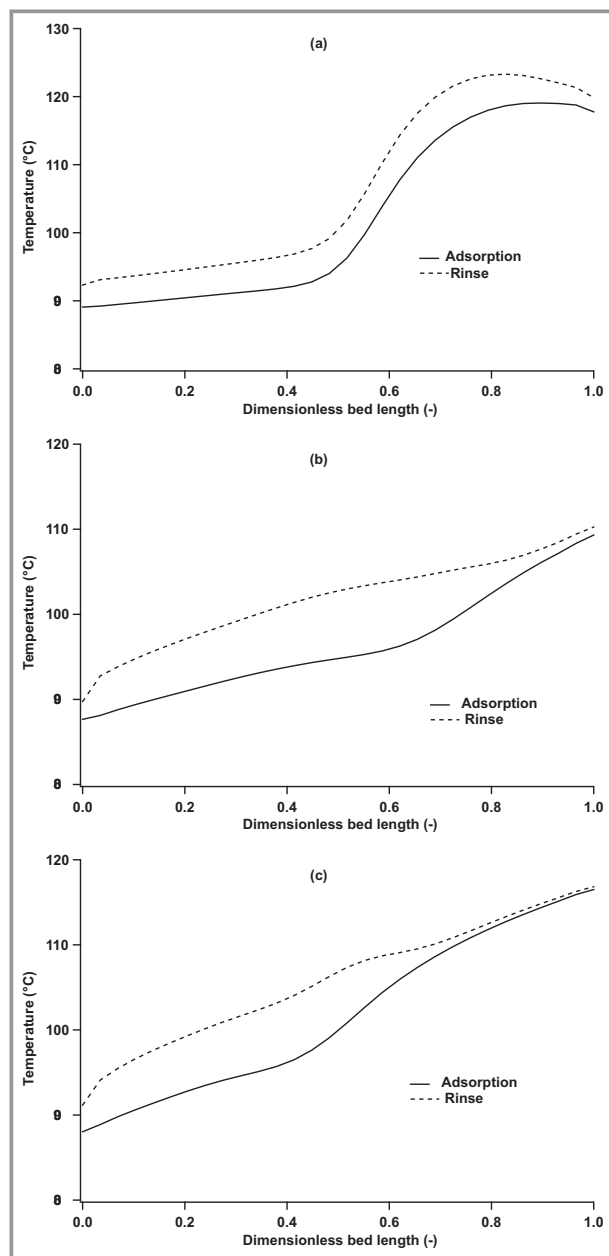


Figure 10. Temperature profiles in the adsorption and rinse steps at cyclic steady state for a) amino silane/SiO₂, b) Lewatit and c) PEI/SiO₂.

In this work, we have only used 5% H₂O since isotherms were not measured beyond the above-mentioned partial pressure for the amino silane grafted silica [42]. In reality, at 90°C, the partial pressure of H₂O in the flue gas would be much higher than 0.05 bar. Extrapolating to higher partial pressures would lead to significant errors and therefore, it is necessary to study the competitive adsorption isotherms of CO₂ and H₂O at higher H₂O partial pressures. Doing this experimentally may be time consuming and also has challenges such as condensation of water along the tubings of

the apparatuses due to improper insulation. As an alternative to experiments, molecular simulations can be a useful and less time intensive tool to obtain adsorption isotherms of CO₂ and H₂O in supported amine sorbents [55].

For the process optimization, the kinetic constants obtained for the amino silane grafted silica was fixed for the other sorbents. This is probably one of the reasons why the differences in the performance of PEI/SiO₂ and Lewatit were not significantly different. The use of appropriate kinetics for the different sorbent could help in predicting the true performance of the sorbents considered in this work. An adsorbent with good capacity and fast kinetics is necessary to achieve high productivity values.

From this work, we see that the energy consumption is around 1–1.4 MJ kg⁻¹ and this is on an electric basis. On a thermal basis, this may be close to 4 MJ kg⁻¹. This is comparable with an absorption process with monoethanolamine (MEA) [56], but new solvents are currently being developed that can capture CO₂ at lower energy consumption values [3, 4, 56]. The ranking of these amine grafted sorbents in a six-step cycle is just the preliminary step to understand the performance of these adsorbents in an adsorption process. Further studies are therefore necessary to identify the best cycle configuration for the supported amine sorbents to lower the energy consumption and benchmark adsorption technology with absorption and to improve the productivity of the CO₂ capture process.

5 Conclusions

In this work, the performance of three different supported amine sorbents in a 6-step VSA cycle was studied through detailed process optimization. All these adsorbents were able to achieve 95% CO₂ purity and 90% CO₂ recovery targets. Amino silane grafted silica had the lowest specific energy consumption of 1 MJ kg⁻¹. Lewatit OC showed the best productivity of 0.48 mol m⁻³ ads s⁻¹, followed by PEI grafted silica and amino silane grafted with values of 0.45 and 0.31 mol m⁻³ ads s⁻¹. Although, the PEI grafted silica had the highest capacity, it did not exhibit the best productivity due to its high nonlinearity (λ). To validate this hypothesis, the PEI isotherms were refitted, and a rigorous optimization performed. For the isotherm with the new isotherm data a better performance in terms of energy and productivity was observed. This exercise demonstrated the importance of measuring isotherms up to near saturation conditions by means of experiments or molecular simulations to accurately determine the saturation capacity as well as the nonlinearity of the isotherm. These supported amine sorbents are associated with high heats of adsorption and consequently high temperature swings were observed. This could potentially degrade the CO₂ adsorption capacity with repeated cycling and, hence, in the design of the VSA process the thermal stability of these adsorbents must be taken into consideration.

Supporting Information

Supporting Information for this article can be found under DOI: <https://doi.org/10.1002/cite.202000172>.

The authors would like to thank Dr. Michael Stöcker of SINTEF industry for the invitation to submit this manuscript in the honour of Professor Jens Weitkamp. This work is a part of the 3D CAPS project. The 3D-CAPS project has received funding from RCN (Norway), RVO (The Netherlands) and UEFISCDI (Romania) and is co-funded by the CO₂ Capture Project (CCP) and the European Commission under the Horizon 2020 programme ACT, Grant Agreement No 691712. Discussions with the CCP members are acknowledged.

Symbols used

b_0	[-]	affinity coefficient of the dual-site Langmuir isotherm for sites 1 and 2
C_T	[mol m ⁻³]	total gas phase concentration
c_i	[mol m ⁻³]	gas phase concentration of component i
C_{pg}	[J kg ⁻¹ K ⁻¹]	specific heat capacity of the gas mixture
C_{pa}	[J kg ⁻¹ K ⁻¹]	specific heat capacity of the adsorbed phase
C_{ps}	[J kg ⁻¹ K ⁻¹]	specific heat capacity of the adsorbent
C_{pw}	[J kg ⁻¹ K ⁻¹]	specific heat capacity of the column wall
D_L	[m ² s ⁻¹]	axial dispersion coefficient
ΔH	[J mol ⁻¹]	heat of adsorption
h_i	[W m ⁻² K ⁻¹]	internal heat transfer coefficient
h_0	[W m ⁻² K ⁻¹]	internal heat transfer coefficient
k_z	[W m ⁻¹ K ⁻¹]	axial thermal conductivity of the gas
k_z	[W m ⁻¹ K ⁻¹]	thermal conductivity of the wall
k_i	[s ⁻¹]	linear driving force coefficient
P	[Pa]	total pressure in the system
P_H	[Pa]	high pressure in the adsorption step
P_L	[Pa]	vacuum pressure in the counter-current evacuation step
P_{INT}	[Pa]	vacuum pressure in the co-current evacuation step
P_{ATM}	[Pa]	ambient pressure
q_i	[mol m ⁻³]	solid phase concentration
q_s	[mol m ⁻³]	solid phase concentration at saturation
q_i^*	[mol m ⁻³]	equilibrium solid phase concentration at saturation
R	[J mol ⁻¹ K ⁻¹]	gas constant
r_i	[m]	column internal radius
r_0	[m]	column external radius
r_p	[m]	pellet radius

T	[K]	temperature inside the column
T_W	[K]	wall temperature
T_a	[K]	ambient temperature
t	[s]	time
ΔU	[J mol ⁻¹]	internal energy of adsorption
v	[m s ⁻¹]	interstitial velocity
y_i	[-]	mole fraction of component i
z	[m]	axial dimension

Greek symbols

ε	[-]	bed void fraction
ρ_s	[kg m ⁻³]	density of the adsorbent
ρ_g	[kg m ⁻³]	density of the gas mixture
ρ_w	[kg m ⁻³]	density of the wall
η	[-]	vacuum pump efficiency
Υ	[-]	ratio of the specific heats
μ	[Pa s]	viscosity of gas mixture

Subscripts

ads	adsorption step
cn	Countercurrent
co	Cocurrent
evac	evacuation step
LR	Light reflux step

Abbreviations

PSA	pressure swing adsorption process
TSA	temperature swing adsorption process
VSA	vacuum swing adsorption process

References

- [1] *Global Warming of 1.5°C*, Intergovernmental Panel on Climate Change Geneva **2018**.
- [2] J. C. Abanades, B. Arias, A. Lyngfelt, T. Mattisson, D. E. Wiley, H. Li, M. T. Ho, E. Mangano, S. Brandani, *Int. J. Greenhouse Gas Control* **2015**, *40*, 126–166. DOI: <https://doi.org/10.1016/j.ijggc.2015.04.018>
- [3] M. Campbell, *Energy Procedia* **2014**, *63*, 801–807. DOI: <https://doi.org/10.1016/j.egypro.2014.11.090>
- [4] G. Manzolini, E. Sanchez Fernandez, S. Rezvani, E. Macchi, E. L. V. Goetheer, T. J. H. Vlught, *Appl. Energy* **2015**, *138*, 546–558. DOI: <https://doi.org/10.1016/j.apenergy.2014.04.066>
- [5] L. Ansaloni, J. Salas-Gay, S. Ligì, M. G. Baschetti, *J. Membr. Sci.* **2017**, *522*, 216–225. DOI: <https://doi.org/10.1016/j.memsci.2016.09.024>
- [6] J. Sun, Q. Li, G. Chen, J. Duan, G. Liu, W. Jin, *Sep. Purif. Technol.* **2019**, *217*, 229–239. DOI: <https://doi.org/10.1016/j.seppur.2019.02.036>
- [7] Y. Wang et al. *Energy Procedia* **2017**, *114*, 650–665. DOI: <https://doi.org/10.1016/j.egypro.2017.03.1209>
- [8] S. Sircar, T. C. Golden, *Sep. Sci. Technol.* **2000**, *35* (5), 667–687. DOI: <https://doi.org/10.1081/SS-100100183>

- [9] J. W. Carter, M. L. Wyszynski, *Chem. Eng. Sci.* **1983**, *38*, 1093–1099. DOI: [https://doi.org/10.1016/0009-2509\(83\)80030-X](https://doi.org/10.1016/0009-2509(83)80030-X)
- [10] M. Khurana, S. Farooq, *Chem. Eng. Sci.* **2016**, *152*, 507–515. DOI: <https://doi.org/10.1016/j.ces.2016.06.033>
- [11] N. Wilkins, A. Rajendran, *Adsorption* **2019**, *25*, 115–133. DOI: <https://doi.org/10.1007/s10450-018-00004-2>
- [12] J.-S. Lee, J.-H. Kim, J.-T. Kim, J.-K. Suoh, J.-M. Lee, C.-H. Lee, *J. Chem. Eng. Data* **2002**, *47* (5), 1237–1242. DOI: <https://doi.org/10.1021/je020050e>
- [13] N. Casas, J. Schell, R. Pini, M. Mazzotti, *Adsorption* **2012**, *18* (2), 143–161. DOI: <https://doi.org/10.1007/s10450-012-9389-z>
- [14] C. A. Grande, R. Blom, A. Möller, J. Möllmer, *Chem. Eng. Sci.* **2013**, *89*, 10–20. DOI: <https://doi.org/10.1016/j.ces.2012.11.024>
- [15] H. W. B. Teo, A. Chakraborty, S. Kayal, *Appl. Therm. Eng.* **2017**, *110*, 891–900. DOI: <https://doi.org/10.1016/j.appltherm-leng.2016.08.126>
- [16] J. Hu, Y. Liu, J. Liu, C. Gu, D. Wu, *Microporous Mesoporous Mater.* **2018**, *256*, 25–31. DOI: <https://doi.org/10.1016/j.micromeso.2017.07.051>
- [17] H. Huang, W. Zhang, D. Liu, B. Liu, G. Chen, C. Zhong, *Chem. Eng. Sci.* **2011**, *66*, 6297–6305. DOI: <https://doi.org/10.1016/j.ces.2011.09.009>
- [18] S. Izzaouihda, H. Abou El Makarim, D. M. Benoit, N. Komiha, *J. Phys. Chem. C* **2017**, *121* (37), 20259–20265. DOI: <https://doi.org/10.1021/acs.jpcc.7b04977>
- [19] G. E. Cmarik, J. C. Knox, *48th International Conference on Environmental Systems*, Albuquerque, NM, July **2018**.
- [20] N. S. Wilkins, J. A. Sawada, A. Rajendran, *Adsorption* **2020**, *26* (5), 765–779. DOI: <https://doi.org/10.1007/s10450-020-00199-3>
- [21] D. Xu, P. Xiao, G. Li, J. Zhang, P. Webley, Y. Zhai, *Chin. J. Chem. Eng.* **2012**, *20* (5), 849–855. DOI: [https://doi.org/10.1016/S1004-9541\(12\)60409-1](https://doi.org/10.1016/S1004-9541(12)60409-1)
- [22] G. Li, P. Xiao, J. Zhang, D. Xu, *AIChE J.* **2014**, *60* (2), 673–689. DOI: <https://doi.org/10.1002/aic.14281>
- [23] S. Krishnamurthy, R. Haghpanah, A. Rajendran, S. Farooq, *Ind. Eng. Chem. Res.* **2014**, *53* (37), 14462–14473. DOI: <https://doi.org/10.1021/ie5024723>
- [24] J. Liu, A. I. Benin, A. M. B. Furtado, P. Jakubczak, R. R. Willis, M. D. LeVan, *Langmuir* **2011**, *27* (18), 11451–11456. DOI: <https://doi.org/10.1021/la201774x>
- [25] A. Sayari, Y. Belmabkhout, *J. Am. Chem. Soc.* **2010**, *132* (18), 6312–6314. DOI: <https://doi.org/10.1021/ja1013773>
- [26] Y. Belmabkhout, R. Serna-Guerrero, A. Sayari, *Ind. Eng. Chem. Res.* **2010**, *49* (1), 359–365. DOI: <https://doi.org/10.1021/ie900837t>
- [27] G. Knowles, P. Webley, Z. Liang, A. Chaffee, in *Recent Advances in Post-Combustion Carbon Capture* (Ed: M. I. Attalla), American Chemical Society, Washington, DC **2012**, 177–205. DOI: <https://doi.org/10.1021/bk-2012-1097.ch009>
- [28] N. Mittal, A. Samanta, P. Sarkar, R. Gupta, *Energy Sci. Eng.* **2015**, *3* (3), 207–220. DOI: <https://doi.org/10.1002/ese3.64>
- [29] R. Veneman, N. Frigka, W. Zhao, Z. Li, S. Kersten, D. W. F. Brilman, *Int. J. Greenhouse Gas Control* **2015**, *41*, 268–275. DOI: <https://doi.org/10.1016/j.ijggc.2015.07.014>
- [30] E. E. Ünveren, B. O. Monkul, S. Sarioglan, N. Karademir, E. Alper, *Petroleum* **2017**, *3* (1), 37–50. DOI: <https://doi.org/10.1016/j.petlm.2016.11.001>
- [31] T. Gelles, S. Lawson, A. A. Rownaghi, F. Rezaei, *Adsorption* **2020**, *26* (1), 5–50. DOI: <https://doi.org/10.1007/s10450-019-00151-0>
- [32] M. Hefi, L. Joss, Z. Bjelobrck, M. Mazzotti, *Faraday Discussions* **2016**, *192*, 153–179. DOI: <https://doi.org/10.1039/C6FD00040A>
- [33] A. Zabout, M. C. Romano, S. Cloete, A. Giuffrida, J. Morud, P. Chiesa, S. Amini, *Int. J. Greenhouse Gas Control* **2017**, *60*, 74–92. DOI: <https://doi.org/10.1016/j.ijggc.2017.03.001>
- [34] M. J. Bos, V. Kroeze, S. Sutanto, D. W. F. Brilman, *Ind. Eng. Chem. Res.* **2018**, *57* (32), 11141–11153. DOI: <https://doi.org/10.1021/acs.iecr.8b00768>
- [35] K. N. Pai, J. D. Baboolal, D. A. Sharp, A. Rajendran, *Sep. Purif. Technol.* **2019**, *211*, 540–550. DOI: <https://doi.org/10.1016/j.seppur.2018.10.015>
- [36] W. Zhang, H. Liu, C. Sun, T. C. Drage, C. E. Snape, *Chem. Eng. J.* **2014**, *251*, 293–303. DOI: <https://doi.org/10.1016/j.ces.2014.04.063>
- [37] M. Khurana, S. Farooq, *AIChE J.* **2017**, *63* (7), 2987–2995. DOI: <https://doi.org/10.1002/aic.15602>
- [38] T. D. Burns, K. N. Pai, S. G. Subraveti, S. P. Collins, M. Krykunov, A. Rajendran, T. K. Woo, *Environ. Sci. Technol.* **2020**, *54* (7), 4536–4544. DOI: <https://doi.org/10.1021/acs.est.9b07407>
- [39] S. Choi, M. L. Gray, C. W. Jones, *ChemSusChem* **2011**, *4* (5), 628–635. DOI: <https://doi.org/10.1002/cssc.201000355>
- [40] A. Abdollahi-Govar, A. D. Ebner, J. A. Ritter, *Energy Fuels* **2015**, *29* (7), 4492–4502. DOI: <https://doi.org/10.1021/acs.energyfuels.5b01119>
- [41] J. W. Dijkstra, S. Walspurger, G. D. Elzinga, J. A. Z. Pieterse, J. Boon, W. G. Haije, *Ind. Eng. Chem. Res.* **2018**, *57* (4), 1245–1261. DOI: <https://doi.org/10.1021/acs.iecr.7b03552>
- [42] S. Krishnamurthy, A. Lind, A. Bouzga, J. Pierchala, R. Blom, *Chem. Eng. J.* **2021**, *406*, 127121. DOI: <https://doi.org/10.1016/j.ces.2020.127121>
- [43] S. Sutanto, J. W. Dijkstra, J. A. Z. Pieterse, J. Boon, P. Hauwert, D. W. F. Brilman, *Sep. Purif. Technol.* **2017**, *184*, 12–25. <https://doi.org/10.1016/j.seppur.2017.04.030>
- [44] K. S. Sánchez-Zambrano, L. L. Duarte, D. A. S. Maia, E. Villarrasa-García, M. Bastos-Neto, E. Rodríguez-Castellón, D. C. S. de Azevedo, *Materials (Basel)* **2018**, *11* (6), 887. DOI: <https://doi.org/10.3390/ma11060887>
- [45] D. Nikolic, E. Kikkiniades, *Adsorption* **2015**, *21*, 283–305. DOI: <https://doi.org/10.1007/s10450-015-9670-z>
- [46] R. Haghpanah, R. Nilam, A. Rajendran, S. Farooq, I. A. Karimi, *AIChE J.* **2013**, *59* (12), 4735–4748. DOI: <https://doi.org/10.1002/aic.14192>
- [47] R. Haghpanah, A. Majumder, R. Nilam, A. Rajendran, S. Farooq, I. A. Karimi, M. Amanullah, *Ind. Eng. Chem. Res.* **2013**, *52* (11), 4249–4265. DOI: <https://doi.org/10.1021/ie302658y>
- [48] S. Krishnamurthy, V. R. Rao, S. Guntuka, P. Sharratt, R. Haghpanah, A. Rajendran, M. Amanullah, I. A. Karimi, S. Farooq, *AIChE J.* **2014**, *60* (5), 1830–1842. DOI: <https://doi.org/10.1002/aic.14435>
- [49] A. Agarwal, L. T. Biegler, S. E. Zitney, *AIChE J.* **2010**, *56* (7), 1813–1828. DOI: <https://doi.org/10.1002/aic.12107>
- [50] R. Todd, J. He, P. A. Webley, C. Beh, S. Wilson, M. A. Lloyd, *Ind. Eng. Chem. Res.* **2001**, *40* (14), 3217–3224. DOI: <https://doi.org/10.1021/ie0008070>
- [51] A. H. Farmahini, D. Friedrich, S. Brandani, L. Sarkisov, *Energy Environ. Sci.* **2020**, *13* (3), 1018–1037. DOI: <https://doi.org/10.1039/C9EE03977E>
- [52] D. Yancy-Caballero, K. T. Leperi, B. J. Bucior, R. K. Richardson, T. Islamoglu, O. K. Farha, F. You, R. Q. Snurr, *Mol. Syst. Des. Eng.* **2020**, *5*, 1205–1218. DOI: <https://doi.org/10.1039/D0ME00060D>
- [53] K. Deb, A. Pratap, S. Agarwal, T. Meyarivan, *IEEE Trans. Evol. Comput.* **2002**, *6* (2), 182–197. DOI: <https://doi.org/10.1109/4235.996017>
- [54] P. Bollini, S. Choi, J. H. Drese, C. W. Jones, *Energy Fuels* **2011**, *25* (5), 2416–2425. DOI: <https://doi.org/10.1021/ef200140z>
- [55] P. Psarras, J. He, J. Wilcox, *Ind. Eng. Chem. Res.* **2017**, *56* (21), 6317–6325. DOI: <https://doi.org/10.1021/acs.iecr.6b05064>
- [56] M. Lucquiaud, J. Gibbins, *Chem. Eng. Res. Des.* **2011**, *89* (9), 1553–1571. DOI: <https://doi.org/10.1016/j.cherd.2011.03.003>